J|A|C|S
ARTICLES
Published on Web 12/29/2007

Local Electronic Structure of Dicarba-*closo*-dodecarboranes $C_2B_{10}H_{12}$

Timothy T. Fister,† Fernando D. Vila,† Gerald T. Seidler,*,† Lukas Svec,†
John C. Linehan,‡ and Julie O. Cross§

Physics Department, University of Washington, Seattle, Washington 98105, Pacific Northwest National Laboratory, Richland, Washington 99352, and Argonne National Laboratory, Argonne, Illinois 60439

Received July 26, 2007; E-mail: seidler@phys.washington.edu

Abstract: We report nonresonant inelastic X-ray scattering (NRIXS) measurement of core−shell excitations from both B 1*s* and C 1*s* initial states in all three isomers of the dicarba-*closo*-dodecarboranes $C_2B_{10}H_{12}$. First, these data yield an experimental determination of the angular-momentum-projected final local density of states (*l*-DOS). We find low-energy resonances with distinctive local *s*- or *p*-type character, providing a more complete experimental characterization of bond hybridization than is available from dipole-transition limited techniques, such as X-ray absorption spectroscopies. This analysis is supported by independent density functional theory and real-space full multiple scattering calculation of the *l*-DOS which yield a clear distinction between tangential and radial contributions. Second, we investigate the isomer sensitivity of the NRIXS signal and compare and contrast these results with prior electron energy loss spectroscopy measurements. This work establishes NRIXS as a valuable tool for borane chemistry, not only for the unique spectroscopic capabilities of the technique but also through its compatibility with future studies in solution or in high-pressure environments. In addition, this work also establishes the real-space full multiple scattering approach as a useful alternative to traditional approaches for excited states calculations of aromatic polyhedral boranes and related systems.

Introduction

Boron's propensity for forming strong, directional, and often exotic chemical bonds is responsible for the great range of interesting examples of and predictions for nanoscale boron-based materials. This includes nanotubes,[1−4] nanowires,[5] two-dimensional sheets,[3,6] clusters of various distinctive symmetries,[4,7−9] and the classic case of polyhedral boranes.[10,11] The issues of aromaticity and delocalization of the bonding state have been key to rationalizing the formation and properties of these substances, and as such this has been a fertile field for the application of a wide range of theoretical approaches.[2,3,6,7,12−15]

The polyhedral boranes exhibit a rich taxonomy of related structures[10,11] that have been extensively studied both experimentally[16] and theoretically.[13,15,17] A unifying characteristic of these molecules is the strong hybridization of atomic states which must result as a consequence of the natural "electron deficiency" of boron and the associated occurrence of three-

† University of Washington.
‡ Pacific Northwest National Laboratory.
§ Argonne National Laboratory.

(1) (a) Boustani, I.; Quandt, A.; Hernandez, E.; Rubio, A. *J. Chem. Phys.* **1999**, *110*, 3176−3185. (b) Ciuparu, D.; Klie, R. F.; Zhu, Y. M.; Pfefferle, L. *J. Phys. Chem. B* **2004**, *108*, 3967−3969. (c) Quandt, A.; Boustani, I. *ChemPhysChem* **2005**, *6*, 2001−2008.
(2) Boustani, I.; Quandt, A.; Rubio, A. *J. Solid State Chem.* **2000**, *154*, 269−274.
(3) (a) Kunstmann, J.; Quandt, A. *Phys. Rev. B* **2006**, *74*, 035413. (b) Lau, K. C.; Pati, R.; Pandey, R.; Pineda, A. C. *Chem. Phys. Lett.* **2006**, *418*, 549−554.
(4) Marques, M. A. L.; Botti, S. *J. Chem. Phys.* **2005**, *123*, 014310.
(5) (a) Cao, L. M.; Zhang, Z.; Sun, L. L.; Gao, C. X.; He, M.; Wang, Y. Q.; Li, Y. C.; Zhang, X. Y.; Li, G.; Zhang, J.; Wang, W. K. *Adv. Mater.* **2001**, *13*, 1701−1704. (b) Otten, C. J.; Lourie, O. R.; Yu, M. F.; Cowley, J. M.; Dyer, M. J.; Ruoff, R. S.; Buhro, W. E. *J. Am. Chem. Soc.* **2002**, *124*, 4564−4565. (c) Wang, D. W.; Lu, J. G.; Otten, C. J.; Buhro, W. E. *Appl. Phys. Lett.* **2003**, *83*, 5280−5282. (d) Wang, Y. Q.; Duan, X. F. *Appl. Phys. Lett.* **2003**, *82*, 272−274. (e) Yang, Q.; Sha, J.; Wang, L.; Yuan, Z. H.; Yang, D. R. *Eur. Phys. J. B* **2007**, *56*, 35−39.
(6) Lau, K. C.; Pandey, R. *J. Phys. Chem. C* **2007**, *111*, 2906−2912.
(7) (a) Aihara, J.; Kanno, H.; Ishida, T. *J. Am. Chem. Soc.* **2005**, *127*, 13324−13330. (b) Grimes, R. N. *J. Chem. Educ.* **2004**, *81*, 658−672.
(8) Alexandrova, A. N.; Boldyrev, A. I.; Zhai, H. J.; Wang, L. S. *Coord. Chem. Rev.* **2006**, *250*, 2811−2866.
(9) Zhai, H. J.; Kiran, B.; Li, J.; Wang, L. S. *Nat. Mater.* **2003**, *2*, 827−833.
(10) (a) Stibr, B. *Chem. Rev.* **1992**, *92*, 225−250. (b) Williams, R. E. *Inorg. Chem.* **1971**, *10*, 210−214. (c) Williams, R. E. *Chem. Rev.* **1992**, *92*, 177−207.
(11) Bregadze, V. I. *Chem. Rev.* **1992**, *92*, 209−223.
(12) (a) Aihara, J. *J. Am. Chem. Soc.* **1978**, *100*, 3339−3342. (b) Chen, Z. F.; King, R. B. *Chem. Rev.* **2005**, *105*, 3613−3642. (c) Cimpoesu, F.; Hirao, K.; Ferbinteanu, M.; Fukuda, Y.; Linert, W. *Monatshefte fur Chemie* **2005**, *136*, 1071−1085. (d) Cyranski, M. K.; Krygowski, T. M.; Katritzky, A. R.; Schleyer, P. V. *J. Org. Chem.* **2002**, *67*, 1333−1338. (e) King, R. B.; Rouvray, D. H. *J. Am. Chem. Soc.* **1977**, *99*, 7834. (f) Park, K.; Pederson, M. R.; Boyer, L. L.; Mei, W. N.; Sabirianov, R. F.; Zeng, X. C.; Bulusu, S.; Curran, S.; Dewald, J.; Day, E.; Adenwalla, S.; Diaz, M.; Rosa, L. G.; Balaz, S.; Dowben, P. A. *Phys. Rev. B* **2006**, 035109. (g) Salam, A.; Deleuze, M. S.; Francois, J. P. *Chem. Phys.* **2003**, *286*, 45−61. (h) Schleyer, P. V.; Najafian, K. *Inorg. Chem.* **1998**, *37*, 3454−3470. (i) Szwacki, N. G.; Sadrzadeh, A.; Yakobson, B. I. *Phys. Rev. Lett.* **2007**, *98*, 166804. (j) Yumatov, V. D.; Il'inchik, E. A.; Volkov, V. V. *Usp. Khim.* **2003**, *72*, 1141−1166.
(13) (a) Buhl, M.; Schleyer, P. V. *J. Am. Chem. Soc.* **1992**, *114*, 477−491. (b) Wales, D. J. *J. Am. Chem. Soc.* **1993**, *115*, 1557.
(14) Hitchcock, A. P.; Wen, A. T.; Lee, S. W.; Glass, J. A.; Spencer, J. T.; Dowben, P. A. *J. Phys. Chem.* **1993**, *97*, 8171−8181.
(15) King, R. B. *Chem. Rev.* **2001**, *101*, 1119−1152.
(16) Venable, T. L.; Hutton, W. C.; Grimes, R. N. *J. Am. Chem. Soc.* **1984**, *106*, 29−37.
(17) Schleyer, P. V.; Najafian, K. *Inorg. Chem.* **1998**, *37*, 3454−3470.

10.1021/ja074794u CCC: $40.75

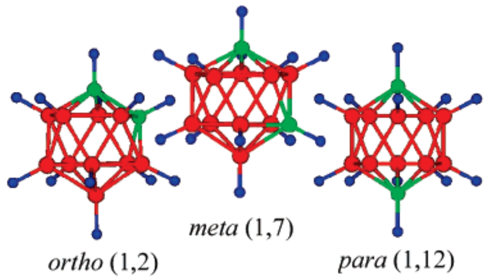

Figure 1. From left to right, *ortho*-, *meta*-, and *para*-$C_2B_{10}H_{12}$. The solid lines signify only nominal geometric proximity, not bonding characteristics.

center bonds, wherein the bonding electron density is often localized in the central region between three boron atoms.[18] The dicarba-*closo*-dodecarboranes, i.e., the quasi-icosahedral $C_2B_{10}H_{12}$ isomers (see Figure 1), are the best-known carboranes and have long been noted for their remarkable stability and diverse applications.[8,11,19−26] For example, the $C_2B_{10}H_{12}$ isomers are now being used in contemporary research in boron neutron capture cancer therapy,[20] HIV inhibitors,[19] superacids,[23] nonlinear optics,[25] molecular transistors,[26] liquid crystals,[22] and functional macromolecular nanomaterials.[21,27]

Here we report measurements of the nonresonant inelastic X-ray scattering (NRIXS) from the three isomers of $C_2B_{10}H_{12}$. Focusing on the contribution to the NRIXS from the core−shell electrons, typically called the nonresonant X-ray Raman scattering (XRS), we find a bulk-sensitive experimental determination of the angular-momentum projected final density of states (i.e, the *l*-DOS) for the B site in *para*-$C_2B_{10}H_{12}$. This relatively new experimental capability yields a more complete characterization of the unoccupied electronic states of the system than is available from traditional dipole-transition limited measurements such as X-ray absorption spectra or electron-energy loss spectra at lower momentum transfers.

By combining the experimental *l*-DOS with independent density functional theory (DFT) and real space full multiple scattering (RSFMS) calculations we find an unambiguous fingerprint of the separation of skeletal and radial bonding in this spectroscopy of the low-lying intramolecular unoccupied states. While our results are specific to $C_2B_{10}H_{12}$, our methodology should be generically applicable across the higher-symmetry members of the polyhedral aromatic boranes and also applicable to other high-symmetry systems with a strong hybridization of states of different orbital angular momentums.

We also return to the problem of the nominal binding energies of the core−shell electrons for both B and C in the three isomers of $C_2B_{10}H_{12}$. We compare and contrast our results with prior gas-phase measurements of core−shell electron energy loss spectra[14,28] (EELS) and with prior theoretical calculations.[14] Additional RSFMS calculations again show good agreement with experiment, further validating this computational approach for the carboranes.

Nonresonant X-ray Raman Scattering

Nonresonant X-ray Raman scattering (XRS) is the contribution to NRIXS wherein the energy lost by X-rays during the scattering process promotes a core electron to an unoccupied final state.[29,30] The development of the third-generation X-ray synchrotrons and of multielement XRS spectrometers has led to an explosive growth in applications of this technique as a bulk-sensitive alternative to and extension of soft X-ray measurements of X-ray absorption fine structure.[29,31−37] Restricting ourselves to polycrystalline or amorphous materials so that one may average the direction of the momentum transfer $\vec{q}$ of the scattering process, the double-differential cross-section for this process is proportional to $S(q,\omega)$, i.e.,

(18) He, J. L.; Wu, E. D.; Wang, H. T.; Liu, R. P.; Tian, Y. J. *Phys. Rev. Lett.* **2005**, *94*, 015504.
(19) Cigler, P.; Kozisek, M.; Rezacova, P.; Brynda, J.; Otwinowski, Z.; Pokorna, J.; Plesek, J.; Gruner, B.; Doleckova-Maresova, L.; Masa, M.; Sedlacek, J.; Bodem, J.; Krausslich, H. G.; Kral, V.; Konvalinka, J. *Proc. Natl. Acad. Sci. U.S.A.* **2005**, *102*, 15394−15399.
(20) Hawthorne, M. F.; Maderna, A. *Chem. Rev.* **1999**, *99*, 3421−3434.
(21) (a) Hawthorne, M. F.; Zink, J. I.; Skelton, J. M.; Bayer, M. J.; Liu, C.; Livshits, E.; Baer, R.; Neuhauser, D. *Science* **2004**, *303*, 1849−1851. (b) Muller, J.; Base, K.; Magnera, T. F.; Michl, J. *J. Am. Chem. Soc.* **1992**, *114*, 9721−9722.
(22) Kaszynski, P.; Douglass, A. G. *J. Organomet. Chem.* **1999**, *581*, 28−38.
(23) Reed, C. A. *Acc. Chem. Res.* **1998**, *31*, 133−139.
(24) (a) McIlroy, D. N.; Zhang, J. D.; Dowben, P. A.; Heskett, D. *Mater. Sci. Eng. A* **1996**, *217*, 64−68. (b) Zhang, J.; McIlroy, D. N.; Dowben, P. A.; Zeng, H.; Vidali, G.; Heskett, D.; Onellion, M. *J. Phys. Condens. Matter* **1995**, *7*, 7185−7194.
(25) Murphy, D. M.; Mingos, D. M. P.; Haggitt, J. L.; Powell, H. R.; Westcott, S. A.; Marder, T. B.; Taylor, N. J.; Kanis, D. R. *J. Mater. Chem.* **1993**, *3*, 139−148.
(26) Soldatov, E. S.; Khanin, V. V.; Trifonov, A. S.; Presnov, D. E.; Yakovenko, S. A.; Khomutov, G. B.; Gubin, C. P.; Kolesov, V. V. *JETP Lett.* **1996**, *64*, 556−560.
(27) Yang, X. G.; Jiang, W.; Knobler, C. B.; Hawthorne, M. F. *J. Am. Chem. Soc.* **1992**, *114*, 9719−9721.
(28) Hitchcock, A. P., et al. *J. Phys. Chem. B* **1997**, *101*, 3483−3493.
(29) Bergmann, U.; Glatzel, P.; Cramer, S. P. *Microchem. J.* **2002**, *71*, 221−230.
(30) Soininen, J. A.; Ankudinov, A. L.; Rehr, J. J. *Phys. Rev. B* **2005**, *72*, 45136.
(31) (a) Tohji, K.; Udagawa, Y. *Phys. Rev. B* **1987**, *36*, 9410−9412. (b) Mao, W. L.; Mao, H. K.; Meng, Y.; Eng, P. J.; Hu, M. Y.; Chow, P.; Cai, Y. Q.; Shu, J. F.; Hemley, R. J. *Science* **2006**, *314*, 636−638. (c) Wernet, P.; Testemale, D.; Hazemann, J. L.; Argoud, R.; Glatzel, P.; Pettersson, L. G. M.; Nilsson, A.; Bergmann, U. *J. Chem. Phys.* **2005**, *123*, 154503. (d) Krisch, M. H.; Sette, F.; Masciovecchio, C.; Verbeni, R. *Phys. Rev. Lett.* **1997**, *78*, 2843. (e) Naslund, L. A.; Edwards, D. C.; Wernet, P.; Bergmann, U.; Ogasawara, H.; Pettersson, L. G. M.; Myneni, S.; Nilsson, A. *J. Phys. Chem. A* **2005**, *109*, 5995−6002. (f) Balasubramanian, M.; Johnson, C. S.; Cross, J. O.; Seidler, G. T.; Fister, T. T.; Stern, E. A.; Hamner, C.; Mariager, S. O. *Appl. Phys. Lett.* **2007**, *91*, 031904. (g) Tohji, K.; Udagawa, Y.; Matsushita, T.; Nomura, M.; Ishikawa, T. *J. Chem. Phys.* **1990**, *92*, 3233−3235. (h) Schuelke, W.; Gabriel, K. J.; Berthold, A.; Schulte-Schrepping, H. *Solid State Commun.* **1991**, *79*, 657−660. (i) Macrander, A. T.; Montano, P. A.; Price, D. L.; Kushnir, V. I.; Blasdell, R. C.; Kao, C. C.; Cooper, B. R. *Phys. Rev. B* **1996**, *54*, 305−312. (j) Caliebe, W. A.; Soininen, J. A.; Shirley, E. L.; Kao, C. C.; Hamalainen, K. *Phys. Rev. Lett.* **2000**, *84*, 3907−3910. (k) Gordon, M. L.; Tulumello, D.; Cooper, G.; Hitchcock, A. P.; Glatzel, P.; Mullins, O. C.; Cramer, S. P.; Bergmann, U. *J. Phys. Chem. A* **2003**, *107*, 8512−8520. (l) Mao, W. L.; Mao, H.-K.; Eng, P. J.; Trainor, T. P.; Newville, M.; Kao, C. C.; Heinz, D. L.; Shu, J. F.; Meng, Y.; Hemley, R. J. *Science* **2003**, *302*, 425−427. (m) Meng, Y. et al. *Nat. Mater.* **2004**, *3*, 111−114. (n) Wernet, P.; Nordlund, D.; Bergmann, U.; Cavalleri, M.; Odelius, M.; Ogasawara, H.; Naslund, L. A.; Hirsch, T. K.; Ojamae, L.; Glatzel, P.; Pettersson, L. G. M.; Nilsson, A. *Science* **2004**, *304*, 995−999. (o) Cai, Y. Q. et al. *Phys. Rev. Lett.* **2005**, *94*, 022502. (p) Lee, S. K.; Eng, P. J.; Mao, H. K.; Meng, Y.; Newville, M.; Hu, M. Y.; Shu, J. F. *Nat. Mater.* **2005**, *4*, 851−854. (q) Sternemann, C.; Soininen, J. A.; Huotari, S.; Vanko, G.; Volmer, M.; Secco, R. A.; Tse, J. S.; Tolan, M. *Phys. Rev. B* **2005**, *72*, 035104. (r) Sternemann, H.; Soininen, J. A.; Sternemann, C.; Hämäläinen, K.; Tolan, M. *Phys. Rev. B* **2007**, *75*, 075118. (s) Lee, S. K.; Eng, P. J.; Mao, H.-K.; Meng, Y.; Shu, J. *Phys. Rev. Lett.* **2007**, *98*, 105502. (t) Lazicki, A.; Maddox, B.; Evans, W. J.; Yoo, C.-S.; McMahan, A. K.; Pickett, W. E.; Scalettar, R. T.; Hu, M. Y.; Chow, P. *Phys. Rev. Lett.* **2005**, *95*, 165503−165506.
(32) Hamalainen, K.; Galambosi, S.; Soininen, J. A.; Shirley, E. L.; Rueff, J. P.; Shukla, A. *Phys. Rev. B* **2002**, *65*, 155111.
(33) Sternemann, C.; Volmer, M.; Soininen, J. A.; Nagasawa, H.; Paulus, M.; Enkisch, H.; Schmidt, G.; Tolan, M.; Schulke, W. *Phys. Rev. B* **2003**, *68*, 035111.
(34) Mattila, A.; Soininen, J. A.; Galambosi, S.; Huotari, S.; Vanko, G.; Zhigadlo, N. D.; Karpinski, J.; Hamalainen, K. *Phys. Rev. Lett.* **2005**, *94*, 247003.
(35) Fister, T. T.; Seidler, G. T.; Hamner, C.; Cross, J. O.; Soininen, J. A.; Rehr, J. J. *Phys. Rev. B* **2006**, *74*, 214117.
(36) Fister, T. T.; Seidler, G. T.; Wharton, L.; Battle, A. R.; Ellis, T. B.; Cross, J. O.; Macrander, A. T.; Elam, W. T.; Tyson, T. A.; Qian, Q. *Rev. Sci. Instrum.* **2006**, *77*, 063901.
(37) Galambosi, S.; Knaapila, M.; Soininen, J. A.; Nygard, K.; Huotari, S.; Galbrecht, F.; Scherf, U.; Monkman, A. P.; Hamalainen, K. *Macromolecules* **2006**, *39*, 9261−9266.

$$\frac{d^2\sigma_{XRS}}{d\Omega d\omega} \propto S(q,\omega) = \sum_f |\langle f|e^{iqr}|i\rangle|^2 \, \delta(E_f - E_i + \hbar\omega) \quad (1)$$

The i and f indices refer to the initial and final states and $\hbar\omega$ is the energy loss. For sufficiently small q, $S(q,\omega)$ becomes proportional to the usual X-ray absorption coefficient such as is measured by inherently dipole-limited X-ray absorption spectroscopy (XAS) or in typical EELS studies.[30]

At higher q, the correspondence between XRS and XAS is broken and transitions to dipole-forbidden final states can significantly change the core−shell contribution to $S(q,\omega)$. In the present study, high q data provide sensitivity to s-type final states which are invisible to dipole-transition limited measurements. This key capability allows us to make a more complete characterization of the local electronic structure of the carboranes.

The quantitative connection between the angular-momentum projected local final density of states (l-DOS or $\rho_l(\omega)$) and the q-dependence of XRS for a given initial state has been investigated by Soininen et al.,[30] who find

$$S(q,\omega) = \sum_l S_l(q,\omega) = \sum_l (2l+1)|M_l(q,\omega)|^2 \, \rho_l(\omega) \quad (2)$$

Hence, $S(q,\omega)$ is a linear superposition of the l-DOS, weighted by smoothly varying coefficients[38] (M_l) that depend only on atomic properties. In principle, this formalism provides the means for model-independent determination of $\rho_l(\omega)$ from the experimentally measured $S(q,\omega)$. This was first proposed by Verdrenskii et al.[39]

As with any spectroscopic technique, the experimental determination of l-DOS is valuable only when it addresses issues pertinent to the material of interest. Focusing on those molecules and compounds of light elements where only s- and p-type local symmetries contribute to the low-lying excitated states, this method allows determination of both ρ_0 (i.e., s-DOS) and ρ_1(i.e., p-DOS), whereas soft X-ray XAS or usual EELS studies of K-shell spectra would only be sensitive to ρ_1 due to the dipole selection rule. The additional information provided by ρ_0 allows two general analysis routes.

First, the existing theoretical methods for calculation and interpretation of the X-ray absorption near edge structure may also be applied to ρ_0, thus addressing the same general scientific questions about local structure and chemical bonding but with spectral information that is independent of (in fact orthogonal to) that provided by XAS. The necessary theoretical generalizations have already been made for calculation of $S(q,\omega)$ or the full spectrum of $\rho_l(\omega)$ by real-space full multiple scattering calculations[30] and by approaches based on the Bethe−Salpeter equation.[32−34,40] Work on nondipole contributions to EELS has shown that comparison to molecular-orbital calculations may be used once the correct selection rules are realized,[41] as does more recent work in the NRIXS community.[34,37] Simultaneous fits to the independent information provided by the different l-DOS components would be optimal in this context.

Second, the qualitative value of simultaneous determination of ρ_0 and ρ_1 grows when localized features (i.e., resonances) are present in the near-edge structure, as is indeed generally the case. Any coincidence in weights in the two l-DOS components is a likely signature of hybridization, thus providing model-independent information on the symmetry of the low-lying unoccupied states in the system.

When moving to molecules and compounds with somewhat heavier elements, ρ_2 (i.e., d-DOS) will also begin to contribute to $S(q,\omega)$. Technical issues[42] associated with the additional extraction of ρ_2 may be overcome with sampling of a sufficiently large range of q.[43] The same two analysis routes and range of scientific issues as discussed above may be used here, but one additional point deserves mention. All excited-state spectroscopies are sensitive to so-called final state effects, most prominently including the interaction between the photoelectron and the core-hole. While final states of different symmetry may be measured by XAS using different initial states (e.g., the K- and $L_{2,3}$-edges in Si), the differences in core-hole wavefunctions and in interaction between the core-hole and photoelectron make it problematic to compare the resulting spectra. The final states being observed in the two measurements are projected from fundamentally different DOS. The determination of the full spectrum of ρ_l starting from a *single* initial state eliminates this issue.

For the case of $C_2B_{10}H_{12}$, we expect that only s- and p-type final states are relevant, resulting in the system of linear equations at each energy point in the unknowns ρ_0 and ρ_1 with

$$\begin{aligned} S(q_1,\omega) &= M_0(q_1,\omega)^2\,\rho_0(\omega) + 3M_1(q_1,\omega)^2\,\rho_1(\omega) \\ &\vdots \\ S(q_N,\omega) &= M_0(q_N,\omega)^2\,\rho_0(\omega) + 3M_1(q_N,\omega)^2\,\rho_1(\omega) \end{aligned} \quad (3)$$

one equation provided by each momentum transfer where an energy loss spectrum is measured. From a pragmatic perspective, this expression is only useful if the inverse problem is well-conditioned. At a minimum this requires that M_0 and M_1 have significantly different q- and ω-dependence (as is indeed the case in the near-edge regime), but it is also clearly helpful if measurements are taken at many (i.e., many more than two) different q so as to strongly overspecify the system of equations. This is exactly the situation in the present study, as enabled by recent instrumentation developments.[36] For $B_{10}C_2H_{12}$, we find that a simple least-squares fitting algorithm allows determination of $\rho_l(\omega)$ from the measured spectra and the calculated atomic $M_l(\omega)$ coefficients via eq 3.

Hence, the combination of recent theoretical and experimental progress provides a fundamental improvement in X-ray spectroscopies. Now-practical q-dependent XRS measurements can be inverted to provide experimental determination of the projection of dipole transition-allowed *and* many dipole-forbidden local final electronic states onto an orbital angular momentum basis. This is in contrast to the more limited information in XAS which is sensitive only to dipole transition-allowed final states. XRS has previously been used to determine

(38) Leapman, R. D.; Rez, P.; Mayers, D. F. *J. Chem. Phys.* **1980**, *72*, 1232−1243.
(39) Vedrinskii, R. V.; Kraizman, V. L.; Novakovich, A. A.; Machavariani, G. Y.; Machavariani, V. S. *J. Phys. Condens. Matter* **1994**, *6*, 11045−11056.
(40) Soininen, J. A.; Shirley, E. L. *Phys. Rev. B* **2001**, *64*, 165112.
(41) (a) Francis, J. T.; Turci, C. C.; Tyliszczak, T.; Desouza, G. G. B.; Kosugi, N.; Hitchcock, A. P. *Phys. Rev. A* **1995**, *52*, 4665−4677. (b) Turci, C. C.; Francis, J. T.; Tyliszczak, T.; Desouza, G. G. B.; Hitchcock, A. P. *Phys. Rev. A* **1995**, *52*, 4678−4688.
(42) Soininen, J. A.; Mattila, A.; Rehr, J. J.; Galambosi, S.; Hamalainen, K. *J. Phys. Condens. Matter* **2006**, *18*, 7327−7336.
(43) Fister, T. T. Ph.D. Dissertation, University of Washington, 2007.

the character (i.e., orbital angular momentum) of near-edge resonances in LiF,[32] B_4C,[44] aligned polyfluorene,[37] and MgB_2.[42] Here, we address a different and broader problem: the consequences of bond hybridization, anisotropy, and aromaticity for the final state DOS in the entire near-edge regime for the carboranes.

Materials and Methods

Materials and Sample Stability. Powders of each of the three isomers of $C_2B_{10}H_{12}$ (Aldrich 98%) were pressed into pellets of approximately one-penetration length thickness, and the resulting pellets were oriented perpendicular to the incident X-ray beam for a transmission geometry. During measurement, samples were held in a helium environment to eliminate possible ozone damage resulting from ionization of air by the incident X-ray beam. No systematic effects in repeated energy scans were seen with increasing exposure. In this regard, the use of hard X-rays in XRS is beneficial as $C_2B_{10}H_{12}$ films have been shown to dissociate into a mixture of *ortho*-carborane and a boron carbide phase with exposure to soft X-ray synchrotron radiation.[45]

Instrumentation and Spectroscopic Details. All XRS measurements were performed with the lower energy resolution inelastic X-ray scattering spectrometer (LERIX) user facility[36] at sector 20-ID PNC/XOR of the Advanced Photon Source. The typical incident and scattered X-ray energy is 10 keV, giving a penetration length of over 3 mm for $C_2B_{10}H_{12}$ and ensuring bulk-sensitivity of the measurements. Uncertainty in energy loss calibration is less than 0.1 eV,[35,36] and the energy resolution for the measurements is 1.35 eV. In the present study, LERIX provided simultaneous measurement of $S(q,\omega)$ at ten different momentum transfers q spanning 0.8−10 $Å^{-1}$. This number of independent measurements and the large range in q are sufficient to strongly overdetermine the inverse problem in eq 3. The contributions to the NRIXS from the relevant core shells (i.e., the XRS) were isolated from the valence NRIXS background by simultaneous fitting of the measured total $S(q,\omega)$ to a Pearson function before the relevant absorption edge and the superposition of the Pearson function and the theoretical q-dependent atomic background when far past the absorption edge. The incident flux was $\sim 5 \times 10^{12}$ photons/s. The count rates at the edges and in the underlying valence Compton background were strong functions of momentum transfer. At $q = 2.4$ $Å^{-1}$ we found 1750 and 320 counts/s at the B and C K-edge step on backgrounds of 2360 and 1250 counts/s, respectively. Increasing q to 9.8 $Å^{-1}$ resulted in 3310 and 1730 counts/s at the B and C K-edge step on backgrounds of 7640 and 23600 counts/s, respectively. Following these measurements we found a significant air leak into the He flight path (outside the sample space) of the instrument. This resulted in a decrease in all count rates by a factor of 3.5 compared to present LERIX performance but otherwise has no consequences for the results presented here.

Full Multiple Scattering Calculations. Calculations for NRIXS from the B and C 1*s* orbitals, the associated atomic backgrounds, and the *l*-DOS were performed using a real space full multiple scattering (RSFMS) package.[30,46] This code is an extension of FEFF8.2 which computes the dynamic structure factor with a single particle Greens function using self-consistent muffin-tin potentials.[30,46] The input to the code was a single molecule whose coordinates were given by previous gas-phase diffraction measurements.[47] After extensive testing, the single molecule calculations were found to work best with the default parameters, i.e., using a core-hole given by the final state rule and a Hedin−Lundqvist exchange-correlation potential.

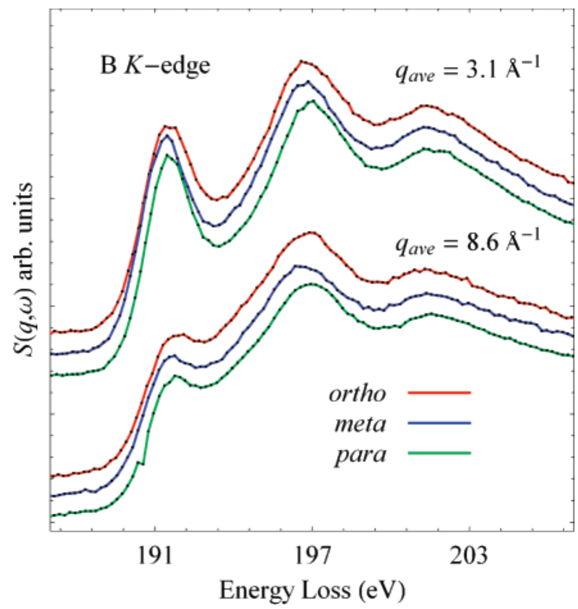

Figure 2. Comparison of the B K-edge for *ortho*-, *meta*-, and *para*-$C_2B_{10}H_{12}$ averaged over low q (top, 3.1 $Å^{-1}$) and high q (bottom, 8.6 $Å^{-1}$).

Density Functional Theory Calculations. The DFT core binding energies were obtained using the Koopman's approximation, i.e., by calculating the difference between the energy of the lowest unoccupied molecular orbital and the average of the core-level energies at each site. This approximation ignores the effect of relaxation upon excitation for both the core and excited-state orbitals, thus resulting in systematically lower binding energies. The theoretical calculations used the B3LYP exchange-correlation functional,[48] the 6-31+G(d,p) basis set,[49] and were performed with Gaussian03.[50] We find that core-optimized basis sets do not change the results significantly. For instance, the EPR-II basis set[51] changed the relative binding energies by less than 0.1 eV. Optimization of the initial structures at the B3LYP/6-31+G(d,p) level also shows very little effect on either the binding energies or $S(q,\omega)$ from the multiple scattering theory. A qualitative *l*-DOS was also obtained within the Koopman's approximation by performing a Natural Atomic Orbital (NAO) population analysis of the B3LYP electron density and producing a histogram of the predominantly *s*-type and *p*-type NAOs.

Results and Discussion

Experimental *l*-DOS Determination for *para*-$C_2B_{10}H_{12}$. In Figure 2, we show a comparison of the B K-edge in the *ortho*-, *meta*-, and *para*-carboranes. Since the signal is an average of the scattering from all 10 boron sites, the isomer-sensitivity is relatively small at both low and high momentum transfers. The XRS spectra are in reasonable agreement with the prior dipole-limit EELS study,[28,52] with the exception of small discrepancies in the exact values and relative shifts of the edge locations. The small negative shift (0.1 eV) in the *meta*-carborane spectrum was found to agree with the isomer-dependence of the DFT-calculated HOMO−LUMO gap. It did not, however, match the

(44) Feng, Y. J.; Seidler, G. T.; Cross, J. O.; Macrander, A. T.; Rehr, J. J. *Phys. Rev. B* **2004**, *69*, 125402.
(45) Byun, D.; Hwang, S.; Zhang, J. D.; Zeng, H.; Perkins, F. K.; Vidali, G.; Dowben, P. A. *Jpn. J. Appl. Phys., Part 2* **1995**, *34*, L941−L944.
(46) Ankudinov, A. L.; Ravel, B.; Rehr, J. J.; Conradson, S. D. *Phys. Rev. B* **1998**, *58*, 7565−7576.
(47) Turner, A. R.; Robertson, H. E.; Borisenko, K. B.; Rankin, D. W. H.; Fox, M. A. *Dalton Trans.* **2005**, 1310−1318.
(48) (a) Becke, A. D. *J. Chem. Phys.* **1993**, *98*, 5648−5652. (b) Lee, C. T.; Yang, W. T.; Parr, R. G. *Phys. Rev. B* **1988**, *37*, 785−789. (c) Miehlich, B.; Savin, A.; Stoll, H.; Preuss, H. *Chem. Phys. Lett*. **1989**, *157*, 200−206.
(49) Francl, M. M.; Pietro, W. J.; Hehre, W. J.; Binkley, J. S.; Gordon, M. S.; Defrees, D. J.; Pople, J. A. *J. Chem. Phys.* **1982**, *77*, 3654−3665.
(50) Frisch, M. J., et al. *Gaussian 03*, revision C.02; Gaussian, Inc.: Wallingford, CT, 2004.
(51) Barone, V. *Recent advances in density functional methods, part I*; World Scientific Publishing Co.: Singapore, 1996.
(52) Hitchcock, A. P.; Wen, A. T.; Lee, S. W.; Glass, J. A.; Spencer, J. T.; Dowben, P. A. *J. Phys. Chem.* **1993**, *97*, 8171−8181.

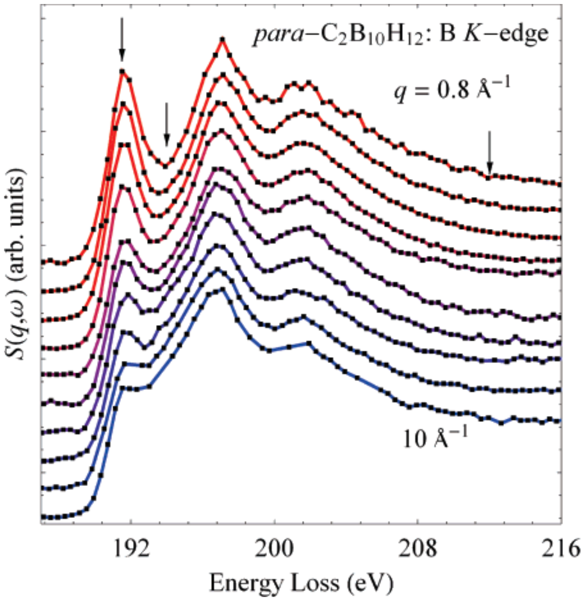

Figure 3. Momentum-transfer (q) dependence of the B 1s nonresonant X-ray Raman scattering (XRS) for *para*-$C_2B_{10}H_{12}$. From top to bottom, the curves correspond to q = 0.8, 2.3, 3.8, 5.2, 6.5, 7.6, 8.6, 9.3, 9.8, and 10.0 Å^{-1}.

binding energy shifts found in previous EELS data,[28,52] where the *meta*-$C_2B_{10}H_{12}$ was shifted forward relative to the other two isomers. The source of this disagreement is unclear but may be due to instrumental issues given its small size.

To simplify the subsequent determination of the l-DOS, we focus on *para*-carborane which has only one unique molecular B site. In Figure 3 we show a more complete view of the q-dependence of the B 1s XRS signal for *para*-$C_2B_{10}H_{12}$. There is substantial q-dependence in the first 10 eV of the near-edge structure; given prior estimates of the ionization threshold,[53] these features correspond to intramolecular bound states. At low q, the spectrum is dominated by dipole-allowed $s \rightarrow p$ transitions, while the higher momentum transfers include additional dipole-forbidden s and, to a much lesser extent, d final states.

In Figure 4 we show linear regression, least-squares fits for the $l = 0$ and 1 components of $S(q,\omega)$ based on eq 3 at the three energy points labeled in Figure 3 (191.5, 194, and 212 eV). Note the narrow 95% confidence interval and the individual contributions from the s- and p-DOS. We find that the d-DOS can be ignored at the 1.5% level.[43] The removal of the valence Compton background from the total NRIXS signal is the primary source of systematic error in the present l-DOS inversion.[42,43] It is of course impossible to characterize such errors when the number of q measurements is only equal to the number of unknown ρ_l. Here, we find that analysis of data collected at a large number of q spanning from the dipole limit to the strong multipole scattering limit allows for straightforward identification of such systematic errors. Spectra plagued by poor background removals will be obvious statistical outliers in the least-squares fit to eq 3 at essentially *all* energy points. In our first attempt to invert eq 3 using data from all 10 experimental q we find that the q = 6.5 Å^{-1} spectrum is a consistent and strong statistical outlier and is, therefore, omitted from the l-DOS inversion procedure. The difficulty with this particular spectrum

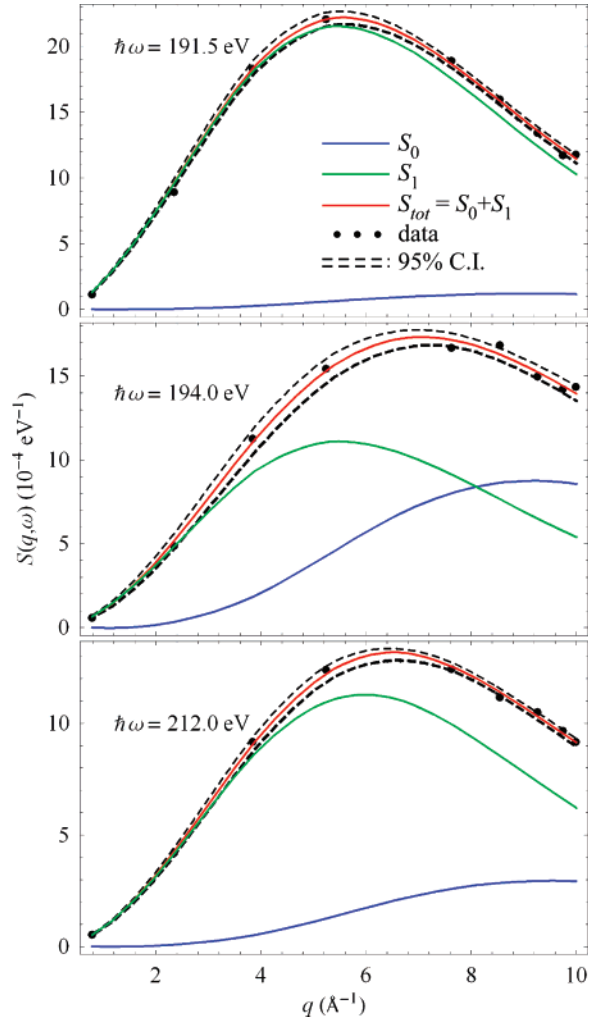

Figure 4. Least-squares fit to the model for $S(q,\omega)$ given in eq 3 compared with data (dots) at the three energy points labeled by arrows in Figure 3. The 95% confidence interval is given by the dashed lines.

is unsurprising: at q = 6.5 Å^{-1} the XRS is close to the peak in the valence Compton scattering contribution to the NRIXS, and as such the extracted XRS spectrum is both most sensitive to a correct treatment of that Compton line shape and also suffers from the lowest count rates relative to background. If the l-DOS inversion was based on only two or three spectra measured at different q, these types of subtle changes in the background-subtracted XRS profiles may go unnoticed. The similarities between M_l coefficients when larger l are considered, for example, M_0 and M_2, will tend to decrease the conditioning of the inverse problem and will again require a larger number of measurements to ensure reliability of the experimentally determined l-DOS.[43]

Hence, by solving eq 3 at each energy point in the near-edge region, we obtain an *experimental* measure of the l-DOS. This result, shown at the top of Figure 5, is compared with an independent theoretical calculation using the modified q-dependent FEFF code, as discussed above.[30] The agreement between the experiment and theory is good, with the small shift in the peak of the s-DOS in the calculation likely due to a strong sensitivity to the radial potential, i.e., to the electron distribution in the B−H radial bonds.

The good agreement between theory and experiment not only serves to additionally validate the l-DOS inversion but also gives

(53) Allison, D. A.; Johansson, G.; Allan, C. J.; Gelius, U.; Siegbahn, H.; Allison, J.; Siegbahn, K. *J. Electron Spectrosc. Relat. Phenom.* **1973**, *1*, 269−83.

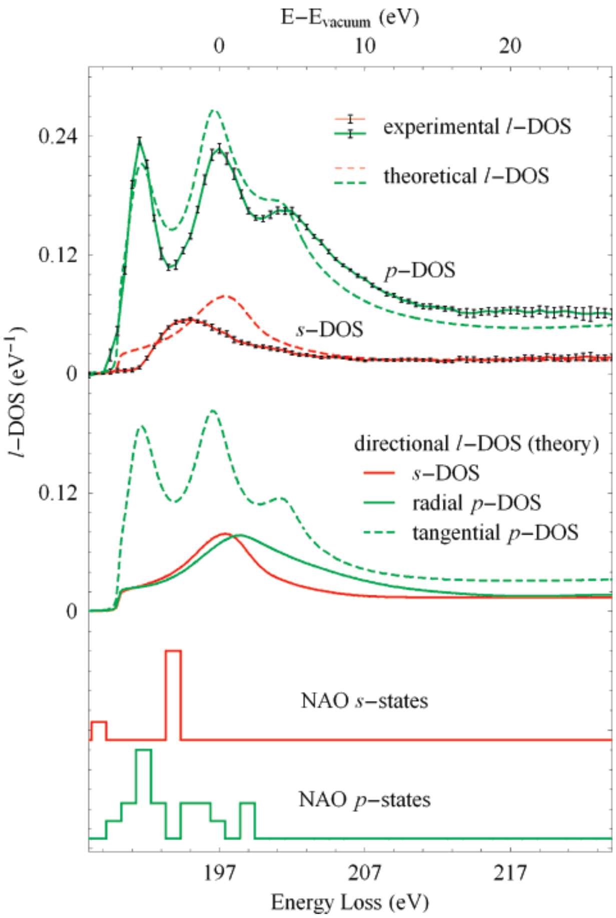

Figure 5. *Top*: The experimentally determined boron *l*-DOS for *para*-$C_2B_{10}H_{12}$, compared to results from real space full multiple scattering calculations. Note the sharp onset of *s*-type character well after the initial, purely *p*-type spectral feature. *Middle*: The directional dependence of the calculated *l*-DOS. Note that the radial (i.e., parallel to the B−H bond) direction contains a single peak near the position of the *s*-DOS. *Bottom*: Qualitative *l*-DOS obtained from a natural atomic orbital (NAO) analysis. The histogram of *s*-type NAO states has been vertically offset from the *p*-states. The bottom axis is the energy loss, and the top axis is the energy of the states with respect to the RSFMS calculated vacuum level at 197 eV. Prior XPS results[53] place the vacuum at 195.6 eV.

some insight into the nature of the relevant states. FEFF performs a real-space full-multiple scattering (RSFMS) calculation based on idealized, spherical muffin-tin potentials. As such, it has inherent difficulty reproducing spectral features at low photoelectron kinetic energy if those features correspond to atomic-like resonances or strongly localized molecular-orbital states; such features would depend sensitively on the use of fully realistic potentials. The general agreement between the FEFF calculations and the experimental *l*-DOS may therefore be a consequence of the delocalization of the final states in this system, which reduces the sensitivity of the RSFMS calculation to the fine details of local anisotropy in any particular atomic potential. Delocalization of the low-lying unoccupied states is expected across a wide range of polyhedral boranes,[15] and as such the RSFMS method may have been underutilized in this field.

Prior analysis, using the tensor spherical harmonic theory (TSH)[15,54] and other approaches,[15] predicts delocalized *p*-type molecular orbitals related to the icosohedra's skeletal (tangential) bonding and *s*−*p* hybridized orbitals related to the radial B−H bonding. To distinguish these types of orbitals we decompose

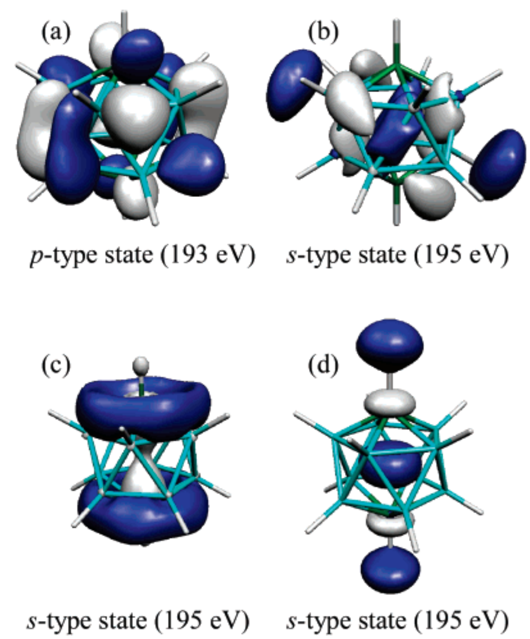

Figure 6. Representative quasi-spherically delocalized virtual molecular orbitals of local *p*-type (a) and *s*-type (b−d) character. In the cage representation of the carborane, the green vertices represent the carbon positions, while the teal vertices correspond to boron atoms.

the RSFMS results onto a spherical harmonic basis, with the molecule oriented so the *z*-direction (i.e., the $Y_{1,0}$ component of the *p*-DOS) is along the radial hydrogen bond from the probe atom. The tangential component is then approximated by the sum of the $Y_{1,-1}$ and $Y_{1,1}$ components of the *p*-DOS. These results are shown in the middle section of Figure 5. We find a clear distinction between the radial and tangential excited states, with the *s*−*p* hybridized radial feature in the calculations matching the experimentally derived *s*-DOS and the *p*-type tangential DOS exhibiting the same characteristic three-peak structure found in the experimental *p*-DOS. This behavior is in agreement with the expectations of TSH, as projected onto the local DOS.

We have also used the previously described DFT approach to further investigate these issues. At the bottom of Figure 5, we show a qualitative *l*-DOS obtained from a Natural Atomic Orbital (NAO) analysis of the DFT density. The NAOs were separated according to their predominantly *s*- or *p*-type character, and the number of states within a certain energy range was counted to form the DOS. Furthermore, the energies were shifted by ∼9 eV to correct for relaxation effects not accounted for within the Koopman's approximation. Despite their qualitative nature, the NAO results mirror the *l*-DOS from experiment and from the RSFMS calculations. They are also in good qualitative agreement with the results reported in Hitchcock et al.,[14] where the dipole-allowed, *p*-character transitions were calculated with a similar approach. In that study, the calculated excitation energies relative to the first dipole-allowed transitions are 4.5 and 6.5 eV, in agreement with the values obtained in the present study (4 and 7 eV, respectively).

Figure 6 shows four typical virtual molecular orbitals which appear significantly analogous to those described in TSH theory. These orbitals are quasi-spherically delocalized, with the devia-

(54) (a) Stone, A. J.; Alderton, M. J. *Inorg. Chem.* **1982**, *21*, 2297−2302. (b) Stone, A. J.; Wales, D. J. *Mol. Phys.* **1987**, *61*, 747.

Table 1. Local Electronic Structure of Dicarba-*closo*-dodecarboranes $C_2B_{10}H_{12}$[a]

	XRS data	EELS data[28]	DFT unoptimized	DFT optimized	charge transfer (e^{-1})
ortho (1,2)	288.42	288.75	279.74	279.48	−0.041
meta (1,7)	287.91 (−0.51)	288.31 (−0.44)	279.17 (−0.57)	278.93 (−0.55)	−0.118
para (1,12)	287.93 (−0.49)	288.07 (−0.68)	279.30 (−0.44)	278.84 (−0.64)	−0.096

[a] For each isomer's C *K*-edge, the XRS and prior EELS[28] edge positions are compared to the DFT results using experimental ("unoptimized") and structurally optimized coordinates. The experimental edge position was determined by fitting the first feature of each spectrum to a Gaussian function. All quantities are reported in eV. The numbers reported in parentheses are the chemical shifts relative to *ortho*-$C_2B_{10}H_{12}$.

tions from the perfect spherical symmetry being caused by the presence of the axial C atoms as well as mixing with the *s* orbitals in the H atoms. From an atomically local perspective their approximate *s* (Figure 6b-d) and *p* (Figure 6a) character can be inferred by the number of nodal planes passing through the reference atom (one for *p* character, none for *s* character). For example, the presence of a local nodal plane at both the C and B atoms can be clearly seen for the orbital shown in Figure 6a. In the case of the orbitals shown in Figure 6b−d, the nodal planes are locate well off the reference atomic positions. Note that the orbital shown in Figure 6a is in good agreement with the excited-state orbitals reported in the prior study of dipole transition-accessible final states.[14]

It would be interesting in the future to extend this discussion to the C sites in $C_2B_{10}H_{12}$. However, this would require improved sensitivity to higher momentum transfer channels of the C K-edge. In the present data, the highest *q* measurements place the C 1*s* XRS on top of the substantially larger background signal from valence Compton scattering. It is also interesting to ask whether the experimentally derived *l*-DOS may more broadly be compared to theory through the use of a best fit to the projection of calculated molecular orbitals onto the atomic sites. Such an approach would be similar to that used by Wales[55] in his discussion of the relationship between cluster (i.e., global) hybridization schemes in TSH theory and the assumed underlying (local) hybridization of atomic orbitals.

Isomer Sensitivity at the C K-Edge. The B K-edge (as shown in Figure 2) shows little or no isomer-sensitivity, owing to the fact that the measured dynamic structure factor is an average of contributions from the 10 boron sites. In contrast, the near-edge structure has considerable isomer-sensitivity for the C 1*s* XRS spectra, as shown in Figure 7. The data in this figure is the average from several momentum transfers with $q_{\mathrm{average}} = 3.1$ Å^{-1}, which is effectively in the dipole limit for the C 1*s* initial state. The shoulder on the low-energy side of the second feature results from the same radial *s*−*p* state discussed above for the B K-edges. This is shown in the directional RSFMS *l*-DOS calculation presented in the bottom of Figure 7. After fitting to a Gaussian, we use the center of the first feature to define the nominal binding energy.

In Table 1, we compare the measured edge position with previous EELS results,[14,28] RSFMS theory, and DFT calculations using experimental[47] and DFT optimized structures. The DFT binding energies were found by the difference between the lowest unoccupied and the average core-level molecular orbital energies, neglecting the effect of orbital relaxation upon excitation. Although this results in systematically lower binding energies, the error is expected to be systematic from isomer to isomer. For lower energy, such as we study here, chemical shifts

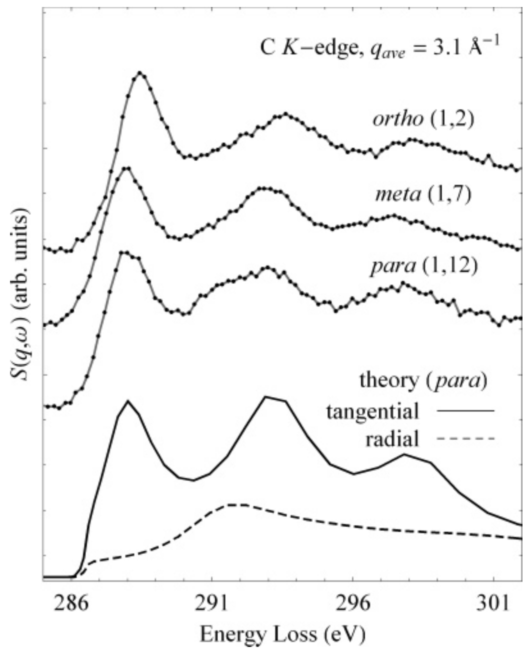

Figure 7. C 1*s* non-resonant X-ray Raman scattering (XRS) for the three isomers of $C_2B_{10}H_{12}$. Directionally dependent, theoretical real space full multiple scattering calculations are shown at the bottom for the *para*-carborane. Note the correspondence of the radial part of $S(q,\omega)$ with the shoulder on the low-energy side of the second feature, which is consistent with the findings from the B K-edge.

can result from core-level (i.e., initial state) or relaxation (i.e., final state) related shifts.[56] In agreement with the analysis of Hitchcock et al.,[28] we find that the relative chemical shift is primarily an initial-state effect. Further support for this position is provided by the lack of correlation between the average calculated valence state of the atom and its relative edge position (i.e., its relative chemical shift). These valence states were the average charge counts in a self-consistent calculation for the single molecule using a real-space multiple scattering code.[46] The disagreement between the present results and the prior EELS work is rather small, ∼0.2 eV, and is comparable to the combined experimental uncertainties in energy loss in the two measurements.

Conclusions

We have used *q*-dependent nonresonant inelastic X-ray scattering to obtain an experimental determination of the unoccupied density of states projected onto the angular momentum basis (*l*-DOS) at the B site for *para*-$C_2B_{10}H_{12}$. This extends prior dipole transition-limited measurements on the carboranes and finds a strong fingerprint of the anisotropic delocalized bonding in the system. We find good performance

(55) Wales, D. J. *Mol. Phys.* **1989**, *67*, 303−320.

(56) Stohr, J. *NEXAFS Spectroscopy*; Springer: Berlin, 1992.

by real-space full multiple scattering calculations, which clearly identify the observed *l*-DOS as being due to distinct skeletal and radial contributions. These conclusions are further supported by DFT calculations of the molecular orbitals of *s*- and *p*-type local character. We also have used the isomer-sensitivity of the C *K*-edge to differentiate between the *ortho*-, *meta*-, and *para*-carboranes. We find good agreement with DFT calculations as regards the relative position of the absorption edge for the three isomers and again find good agreement with the RSFMS calculations. The good performance of the RSFMS method throughout this study suggests that it has been underutilized in calculations of the local electronic structure of aromatic boranes and their derivatives.

Taken *en masse*, our results establish XRS as an important tool for borane chemistry. Our experimental approach is generic and may be readily applied to related polyhedral or planar boranes and their derivatives. Due to the large penetration length of the 10 keV incident X-rays, XRS measurements are incontrovertibly bulk-sensitive and may in the future be adapted to borane chemistry in concentrated gas or solution phases or in extreme conditions such as high pressures.

Acknowledgment. This research was supported by DOE, Basic Energy Science, Office of Science, Contract Nos. DE-FGE03-97ER45628 and W-31-109-ENG-38, ONR Grant No. N00014-05-1-0843, Grant DE-FG03-97ER5623, NIH NCRR BTP Grant RR-01209, the Leonard X. Bosack and Bette M. Kruger Foundation, the Hydrogen Fuel Cell Initiative of DOE Office of Basic Energy Sciences, and the Summer Research Institute Program at the Pacific Northwest National Lab. Battelle operates the Pacific Northwest National Lab for DOE. The operation of Sector 20 PNC-CAT/XOR is supported by DOE Basic Energy Science, Office of Science, Contract No. DE-FG03-97ER45629, the University of Washington, and grants from the Natural Sciences and Engineering Research Council of Canada. Use of the Advanced Photon Source was supported by the U.S. Department of Energy, Basic Energy Sciences, Office of Science, under Contract W-31-109-Eng-38. We thank Mark Lee and Fred Hawthorne for providing some of the samples used in this study. We also thank John Rehr, Aleksi Soininen, Adam Hitchcock, and Ed Stern for stimulating discussions.

Supporting Information Available: Complete author list for ref 31o, the absolute energies and optimized structures from the DFT calculations, and the data presented in Figures 2, 3, and 7. This material is free of charge via the Internet at http://pubs.acs.org.

JA074794U